

Journal Pre-proofs

A Kinetics-Based Model of Fatigue Crack Growth Rate in Bituminous Material

Hui Li, Xue Luo, Yuqing Zhang

PII: S0142-1123(21)00045-1

DOI: <https://doi.org/10.1016/j.ijfatigue.2021.106185>

Reference: JIJF 106185

To appear in: *International Journal of Fatigue*

Received Date: 20 October 2020

Revised Date: 29 January 2021

Accepted Date: 4 February 2021

Please cite this article as: Li, H., Luo, X., Zhang, Y., A Kinetics-Based Model of Fatigue Crack Growth Rate in Bituminous Material, *International Journal of Fatigue* (2021), doi: <https://doi.org/10.1016/j.ijfatigue.2021.106185>

This is a PDF file of an article that has undergone enhancements after acceptance, such as the addition of a cover page and metadata, and formatting for readability, but it is not yet the definitive version of record. This version will undergo additional copyediting, typesetting and review before it is published in its final form, but we are providing this version to give early visibility of the article. Please note that, during the production process, errors may be discovered which could affect the content, and all legal disclaimers that apply to the journal pertain.

© 2021 Published by Elsevier Ltd.



A Kinetics-Based Model of Fatigue Crack Growth Rate in Bituminous Material

Journal Pre-proofs

Hui Li

College of Civil Engineering and Architecture

Zhejiang University

866 Yuhangtang Road, An-zhong Bldg.

Hangzhou 310058, Zhejiang, China

Email: huili94@zju.edu.cn

Xue Luo

(corresponding author)

College of Civil Engineering and Architecture

Zhejiang University

866 Yuhangtang Road,

Hangzhou 310058, Zhejiang, China

Phone: (86) 571-88206542

Email: xueluo@zju.edu.cn

Yuqing Zhang

Aston Institute of Materials Research

Aston University

Aston Triangle, Birmingham, B4 7ET, U.K.

Phone: +44 (0) 121-204-3391

Email: y.zhang10@aston.ac.uk

This study aims to propose a kinetics-based model of the fatigue crack growth rate coupling with temperature, strain level and damage degree for bituminous materials. The fatigue crack length is calculated by the energy-based mechanistic (EBM) approach, and kinetic parameters characterizing the fatigue crack growth rate are determined based on the Arrhenius equation. The results show that the logarithm of fatigue crack growth rate is linear to the inverse of absolute temperature, and the cracking activation energy is independent on strain level and damage degree. Besides, the proposed kinetics-based model can predict fatigue crack growth rate at arbitrary conditions.

Key words: bituminous materials; energy-based mechanistic (EBM) approach; Arrhenius equation; fatigue crack growth rate; cracking activation energy

The fatigue cracking of bituminous mixtures is the most common failure mode of bituminous pavements under the long-term cyclic traffic load, which seriously affects the service performance and life of pavement structures. The cohesive fatigue cracking of bituminous materials is one of the main factors causes the fatigue cracking of bituminous mixtures [1-2]. Therefore, many fatigue indicators, such as, the stiffness or pseudo-stiffness decreasing by 50% [3-4], the phase angle increasing to the peak value [5], or the peak value of $S \times N$ (S is the stiffness and N is the loading cycle) [6] were proposed to evaluate the fatigue behavior for bituminous materials. Besides, some energy dissipation indicators, including the energy ratio (ER) [5][7], the dissipated energy ratio (DER) [8-10], the dissipated energy (DR) [11] and the ratio of dissipated energy change (RDEC) [12-14] were adopted to characterize the fatigue performance of bituminous materials. The Strategic Highway Research Program (SHRP) proposed another important indicator, the fatigue factor $|G^*| \cdot \sin \delta$ ($|G^*|$ is the shear modulus, δ is the phase angle) to quantify the fatigue resistance for bituminous materials [15]. These indicators have been employed in many researches [16-17].

Furthermore, the fatigue crack length indicator was formulated to characterize the fatigue performance of bituminous materials during the fatigue damage process in some studies [18-19], which has a major advantage is that the fatigue crack length indicator can intuitively reflect the damage degree of bituminous materials. However, in these studies, the fatigue crack length under the destructive condition was derived based on the linear viscoelastic constitutive equation under the nondestructive condition, which makes the calculation results inaccurate. Hence, to better understand the fatigue mechanisms, the authors proposed a fatigue crack length model for bituminous materials based on the torque and dissipated strain energy equilibrium principles, and the fatigue crack length model was investigated by the image process method [20-21].

In addition, some researchers studied the fatigue crack growth rate during the fatigue crack propagation process for bituminous materials. Such as, Hintz and Bahia analyzed the fatigue crack growth rate and investigated a fatigue failure criterion for bituminous materials [19], and Shan et al. studied the fatigue crack growth rate for bituminous materials under the controlled-stress and controlled-strain fatigue loading mode based on the torque predictions of the fatigue crack length [18]. Moreover, the pseudo J-integral Paris' law model applicable to the stable fatigue crack growth stage was employed to formulate the fatigue cracking rate for the bituminous materials under the cyclic tensile, compression and shear load [22-24]. Generally, combining the energy release rate caused by the fatigue cracking

and the fatigue crack growth rate can obtain the model parameters, and the results showed that the model parameters are independent of the strain level and loading frequency [21, 23-24]. However, the energy release rate must be known to determine the fatigue crack growth rate based on the pseudo J-integral Paris' law model under an arbitrary condition, i.e., it is closely related to the strain level, temperature, and damage degree.

Therefore, the pseudo J-integral Paris' law model is limited to predict the fatigue crack growth rate for the bituminous materials under different conditions. Thus, the fatigue tests must be performed to obtain the fatigue crack growth rates of bituminous materials at the specific temperature, strain level and damage degree, and it requires a large amount of test time and costs. To better predict the fatigue crack growth rate during the fatigue crack propagation process, based on the results at different damage degrees (seven different fatigue crack lengths) of three types of bituminous materials were tested by the shear fatigue test at different temperatures (15°C, 20°C, 25°C), strain levels (5%, 6%, 7%), this study aims to establish a kinetics-based model of the fatigue crack growth rate for bituminous materials, which can predict the fatigue crack growth rate at different temperatures, strain levels and damage degrees of bituminous materials.

The study is organized as follows. The materials and laboratory tests are first elaborated. Secondly, the shear strain and shear stress models of bituminous materials during the controlled-strain shear fatigue test are constructed. The fatigue crack length model is established by the energy-based mechanistic (EBM) approach and the fatigue crack growth rate is calculated. Thirdly, the kinetic indicators (cracking activation energy and pre-exponential factor) characterizing the fatigue crack growth rate of bituminous materials are solved based on the Arrhenius equation. Then, based on the statistical analysis method, the cracking activation energies of two repeated tests were obtained at three strain levels and seven damage degrees of three types of bituminous materials are analyzed, and the model of the cracking pre-exponential factor is established. In addition, a kinetics-based model of fatigue crack growth rate coupling with temperature, strain level and damage degree is proposed. Finally, a summary section concludes this study with the main results and future work.

2 Materials and Laboratory Tests

2.1 Materials

In this study, three types of bituminous materials are selected, including virgin bituminous binders and bituminous mastics with the two kinds of powder volume contents (10% and 27%), which are denoted as bituminous materials BB, BM₁ and BM₂, respectively. The basic

properties (penetration, softening point and ductility) and specification requirements of the virgin bituminous binder are shown in Table

1. The basic properties of the virgin bituminous binder meet the requirement in the specification, and the SHRP performance grade is PG64-22. In addition, the bituminous mastics are prepared by mixing the virgin bituminous binder and limestone powder. In this study, two different powder volume contents are adopted. The powder volume content of 27% (i.e. the mass ratio between the powder and virgin bituminous binders is 1) represents the typical ratio of powder and bituminous binders in asphalt pavements. Besides, to study the following model parameters, 10% of powder volume content (i.e. the mass ratio of between the powder and bituminous binders is 0.3) is added. The main component of the limestone powder is calcium carbonate, and its basic properties (relative density, water content and hydrophilic coefficient) and the specification requirements are shown in Table 1. The basic properties of the limestone powder also meet the requirement in the specification.

Table 1 Basic properties and requirements of bituminous binders and limestone powder

Materials	Properties	Units	Requirements	Results
Bituminous binders	Penetration at 25°C	0.1mm	60-80	66
	Softening point	°C	46	49.0
	Ductility at 15°C	cm	≥100	>100
Limestone powder	SHRP performance grade		PG64-22	
	Relative density	g/cm ³	≥2.50	2.765
	Water content	%	≤1	0.49
	Hydrophilic coefficient	-	<1	0.68

2.2 Equipment and Sample Preparation

The experimental equipment used in this study is the Discovery Hybrid Rheometer of TA Instruments. All of fatigue tests include three temperatures: 15°C, 20°C and 25°C. The diameter of the selected parallel plate is 8mm. In this way, when performing the fatigue test, the diameter and height of the bituminous sample are 8mm and 2mm respectively. In addition, in order to avoid uneven temperature distribution within the bituminous samples, they need to be heated to the target temperature of the fatigue test. Then, turn off the instrument environment furnace so that the sample is kept at the target temperature for 5 minutes.

When the bituminous samples are ready, the fatigue test (i.e. destructive time sweep test) is carried out on the bituminous sample. Then, the shear modulus and phase angle at the crack growth stage are recorded. In addition, all of destructive time sweep tests of the bituminous materials are conducted at three temperatures (15°C, 20°C, 25°C) and one loading frequency (10 Hz) and 5%, 6% and 7% of strain levels are selected as the destructive strain levels, respectively. Repeated tests are performed on the three bituminous materials under each test condition. When the deviation between the two measured results is greater than 10%, the third test is repeated and the final test results are averaged.

Finally, the relationship between the shear modulus, phase angle of the bituminous materials and loading time can be obtained after performing destructive time sweep tests. Taking the bituminous material BB as an example, Fig. 1 shows the typical curve of the shear modulus and phase angle at 5% of strain level, 20°C and 10 Hz. It can be seen from Fig. 1 that the shear modulus decreases with the increase of loading time. The phase angle first increases to the peak and then decreases with the increase of loading time. Besides, the shear modulus is close to zero and the value of the phase angle oscillates within a certain range at the later loading stage, which indicates that the bituminous materials BB is close to completely damaged.

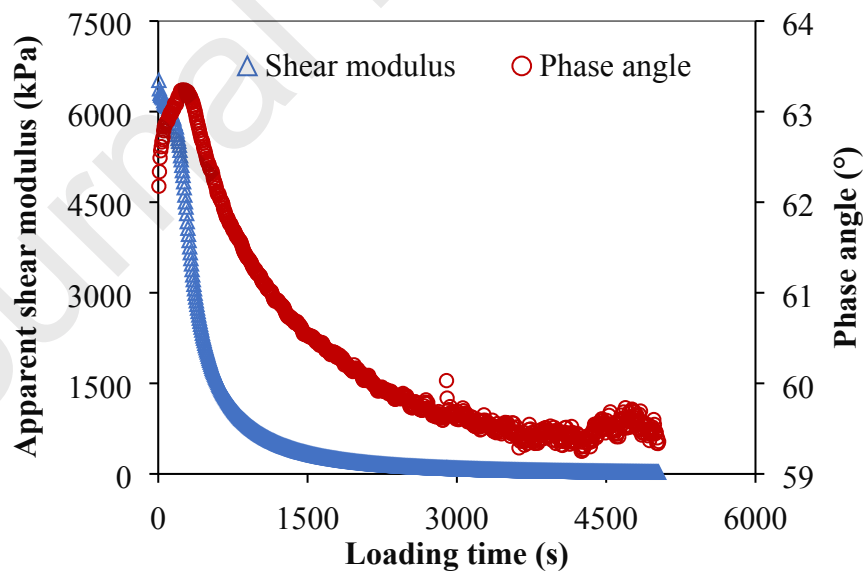


Fig. 1. Shear modulus and phase angle of the bituminous material BB at 5% of strain level, 20°C and 10 Hz

3 Determination of the Fatigue Crack Length and Crack Growth Rate

To calculate the fatigue crack growth rate of bituminous materials when performing the controlled-strain shear fatigue test, the shear

strain and shear stress models are first established in this section. Then, the torque, dissipated strain energy and recoverable strain energy

of bituminous materials are calculated. Furthermore, the fatigue crack length and the fatigue crack growth rate of bituminous materials are calculated based on the EBM approach. The details are introduced step by step.

3.1 Establishment of the Shear Strain and Shear Stress Models

When the destructive time sweep test is carried out on the bituminous materials, fatigue cracks gradually generate and expand to the loading center of the sample with the increase of loading cycle [20-21]. In this study, the entire bituminous material sample containing edge fatigue crack is defined as the apparent material, while the central nondestructive material without edge crack is defined as the intact material. Fig.2 shows the distribution of the shear strain and shear stress of the apparent material and intact material of the bituminous material sample when performing the destructive time sweep test.

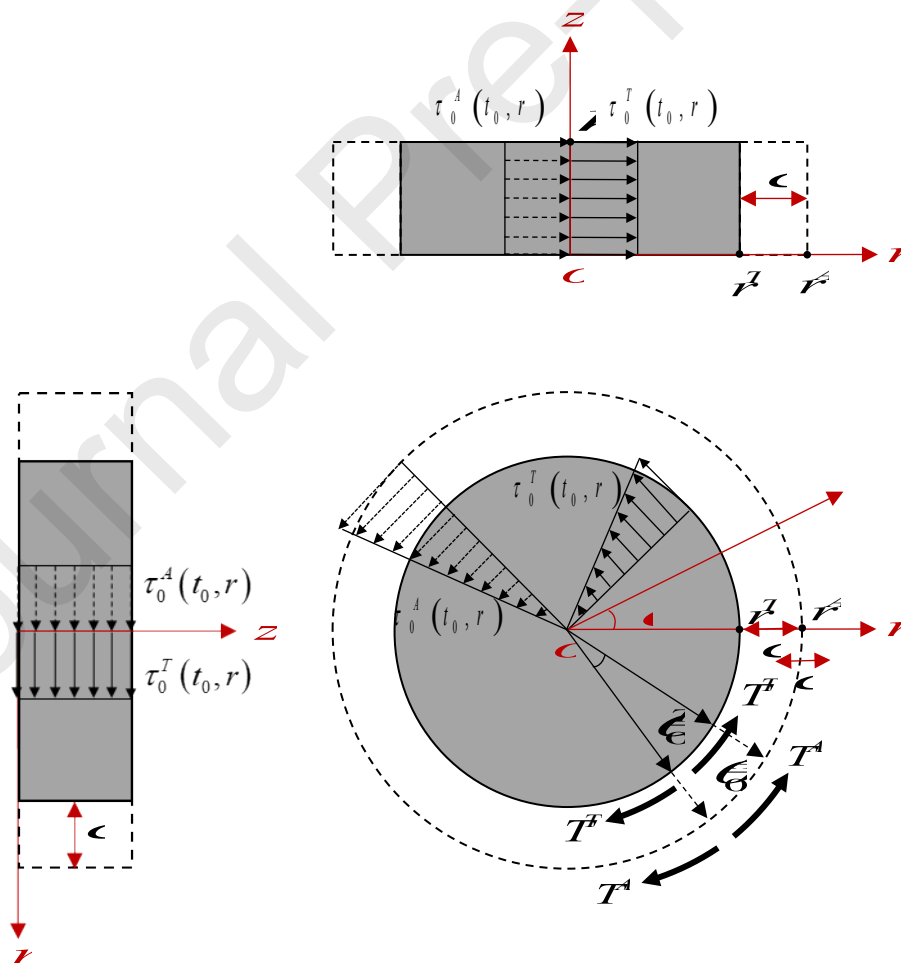


Fig.2. Distribution of the shear strain and shear stress of the apparent material and intact material of the bituminous material sample when performing the destructive time sweep test

Next, the distribution functions of the shear strain and stress of the apparent material and intact material are established. For the apparent material, the apparent shear strain is modeled by the following equation:

$$\gamma^A(t, r) = \gamma_0^A(t_0, r) \sin(\omega t) = \frac{\theta_0^A}{h} r \sin(\omega t) \quad (1)$$

where $\gamma^A(t, r)$ is apparent shear strain at arbitrary loading time t ($t \in [t_0, t_0 + 2\pi / \omega]$) and radius r ; $\gamma_0^A(t_0, r)$ is apparent shear strain amplitude at arbitrary initial loading time t_0 and radius r ; ω is loading frequency; θ_0^A is apparent rotation angle of the test; and h is the height of the sample. These variables are marked in Fig. 2 and Fig. 3a. The superscript ‘‘A’’ represents the variable of the apparent material, while the superscript ‘‘T’’ represents the variable of the intact material.

As a typical viscoelastic material, the shear strain of the bituminous material lags behind the shear stress. As shown in Fig.3a, the apparent phase δ^A can quantify the time lag of the shear strain. Therefore, the apparent shear stress can be modeled as below:

$$\tau^A(t, r) = \tau_0^A(t_0, r) \sin(\omega t + \delta^A) = \frac{r}{r^A} \tau_0^A(t_0, r^A) \sin(\omega t + \delta^A) \quad (2)$$

where $\tau^A(t, r)$ is apparent shear stress at arbitrary loading time t and radius r ; $\tau_0^A(t_0, r)$, $\tau_0^A(t_0, r^A)$ are apparent shear stress amplitude at arbitrary initial loading time t_0 and radius r , apparent radius r^A , respectively.

The apparent shear modulus $|G^{*A}|$ is calculated by:

$$|G^{*A}| = \frac{\tau_0^A(t_0, r)}{\gamma_0^A(t_0, r)} \quad (3)$$

Then, the apparent torque, dissipated strain energy and recoverable strain energy of bituminous materials are calculated. The total apparent torque $T^A(t_0)$ at loading time t_0 can be calculated by carrying on the triple integral over the entire apparent volume for the apparent torque $T^A(t_0, r)$ at any loading time t_0 and radius r :

$$T^A(t_0) = \iiint_{V^A} T^A(t_0, r) dV = \int_0^{r^A} \tau_0^A(t_0, r) \cdot 2\pi r \cdot dr \cdot r \quad (4)$$

In addition, the strain energy hysteresis loop composed of the shear stress and shear strain is shown in Fig.3b. The area within the strain energy hysteresis loop composed of the apparent shear stress and shear strain at any loading time t_0 and radius r stands for apparent dissipated strain energy $DSE^A(t_0, r)$. Then, the triple integral over the entire apparent volume for $DSE^A(t_0, r)$ can be conducted to obtain the total $DSE^A(t_0)$ as below:

$$DSE^A(t_0) = \iiint DSE^A(t_0, r) dV = 2\pi^2 h \sin \delta^A \int_0^{r^A} \tau_0^A(t_0, r) \gamma_0^A(t_0, r) r dr \quad (5)$$

Journal Pre-proofs

Besides, at any loading time t_0 and radius r , two parts of apparent recoverable strain energy $RSE^A(t_0, r)$ are concluded as shown in Fig

3b. Performing a triple integral over the entire apparent volume for $RSE^A(t_0, r)$ can calculate total $RSE^A(t_0)$ as follows:

$$RSE^A(t_0) = \iiint_{V^A} RSE^A(t_0, r) dV = 2\pi h \left(-\frac{\sin \delta^A (2\delta^A + \sin(2\delta^A) - \pi)}{2} - \cos^3(\delta^A) \right) \int_0^{r^A} \tau_0^A(t_0, r) \gamma_0^A(t_0, r) r dr \quad (6)$$

For the intact material, similarly, the true shear strain is modeled by:

$$\gamma^T(t, r) = \gamma_0^T(t_0, r) \sin(\omega t) = \frac{\theta_0^T}{h} r \sin(\omega t) \quad (7)$$

in which $\gamma^T(t, r)$ is true shear strain at arbitrary loading time t and radius r ; $\gamma_0^T(t_0, r)$ is true shear strain amplitude at arbitrary initial loading time t_0 and radius r ; and θ_0^T is true rotation angle.

Thus, the true shear stress can be modeled by the following function:

$$\tau^T(t, r) = \tau_0^T(t_0, r) \sin(\omega t + \delta^T) = \frac{r}{r^T} \tau_0^T(t_0, r^T) \sin(\omega t + \delta^T) \quad (8)$$

where $\tau^T(t, r)$ is true shear stress at arbitrary loading time t and radius r ; $\tau_0^T(t_0, r)$, $\tau_0^T(t_0, r^T)$ are true shear stress amplitude at arbitrary initial loading time t_0 and radius r , true radius r^T , respectively; and δ^T is true phase angle.

The true shear modulus $|G^{*T}|$ can be determined by:

$$|G^{*T}| = \frac{\tau_0^T(t_0, r)}{\gamma_0^T(t_0, r)} \quad (9)$$

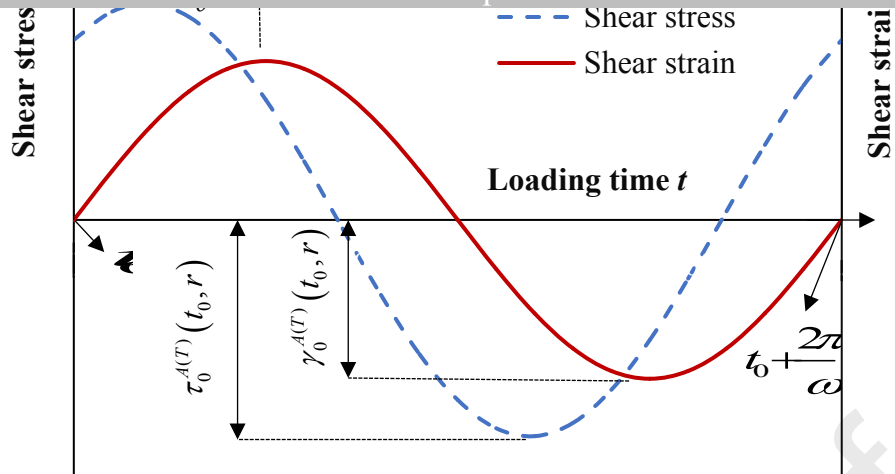
Finally, the true torque $T^T(t_0)$, true dissipated strain energy $DSE^T(t_0)$ and true recoverable strain energy $RSE^T(t_0)$ of bituminous materials at any loading time t_0 can be determined by performing the triple integral over the entire true volume. The $T^T(t_0)$, $DSE^T(t_0)$ and $RSE^T(t_0)$ are calculated by the following three equations, respectively:

$$T^T(t_0) = \iiint_{V^T} T^T(t_0, r) dV = \int_0^{r^T} \tau_0^T(t_0, r) \cdot 2\pi r \cdot dr \cdot r \quad (10)$$

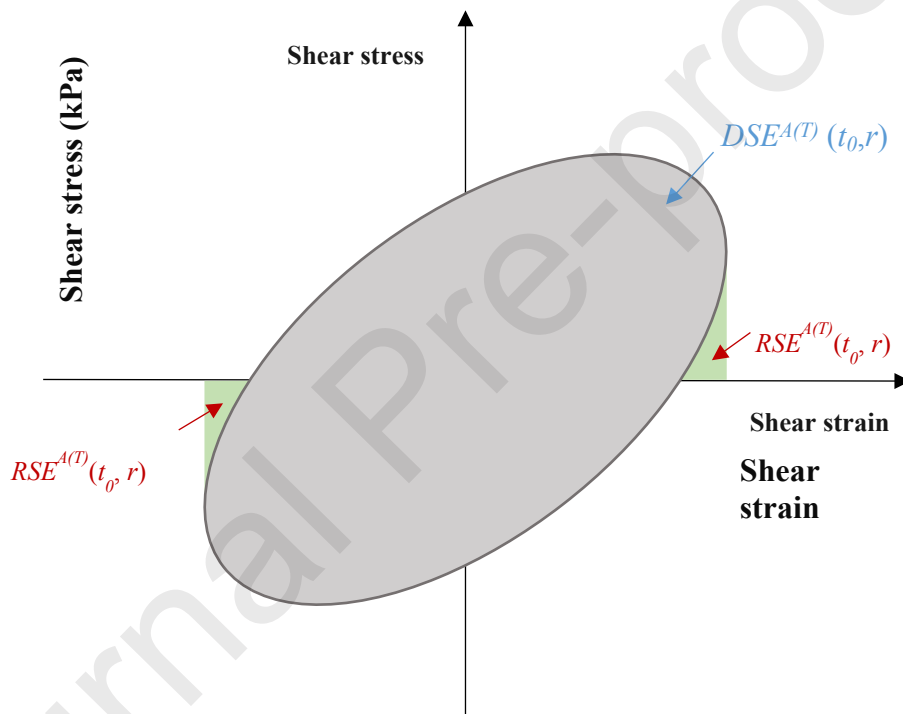
$$DSE^T(t_0) = \iiint_{V^T} DSE^T(t_0, r) dV = 2\pi^2 h \sin \delta^T \int_0^{r^T} \tau_0^T(t_0, r) \gamma_0^T(t_0, r) r dr \quad (11)$$

$$RSE^T(t_0) = \iiint_{V^T} RSE^T(t_0, r) dV = 2\pi h \left(-\frac{\sin \delta^T (2\delta^T + \sin(2\delta^T) - \pi)}{2} - \cos^3(\delta^T) \right) \int_0^{r^T} \tau_0^T(t_0, r) \gamma_0^T(t_0, r) r dr \quad (12)$$

where $T^T(t_0, r)$, $DSE^T(t_0, r)$ and $RSE^T(t_0, r)$ are the true torque, dissipated strain energy and recoverable strain energy at any loading time t_0 and radius r , respectively.



a. Schematic diagram of the apparent or true shear stress and shear strain at any radius within a loading cycle



b. Schematic diagram of the strain energy hysteresis loop composed of the apparent or true shear stress and shear strain at any radius

Fig.3. Schematic diagram of the apparent or true shear stress, shear strain and strain energy hysteresis loop at any radius of bituminous materials

3.2 Computation of Fatigue Crack Parameters

The authors have studied the fatigue damage evolution and healing of bituminous mixtures under the fatigue load based on the EBM approach [25-27]. In this study, controlled-strain shear fatigue tests are conducted for bituminous materials. The torque and dissipated strain energy balance principles can be used to solve the fatigue crack length of bituminous materials, which are expressed as follows:

$$\frac{T^A - T^T}{\text{Journal Pre-proofs}} \quad (13)$$

$$DSE^A = DSE^T \quad (14)$$

$$RSE^A = RSE^T \quad (15)$$

Substituting Eqs. (4), (10) into Eq. (13) and substituting Eqs. (5), (6), (11), (12) into Eqs. (14), (15), then simultaneous solving Eqs. (13), (14), (15). The true radius r^T of bituminous materials can be obtained when performing the controlled-strain shear fatigue test [20]:

$$r^T = \left(\frac{|G^{*A}|}{|G^{*T}|} \right)^{1/4} r^A \quad (16)$$

In this way, the fatigue crack length c of bituminous materials can be calculated by the following formula:

$$c = r^A - r^T \quad (17)$$

The surface of bituminous materials showed different characteristics at different areas after performing the time sweep test under high oscillation shear strain levels, and an image processing approach was performed to validate Eqs (16) and (17) in our previous study [20].

The calculated fatigue crack length and measured fatigue crack length were compared, and the two are close.

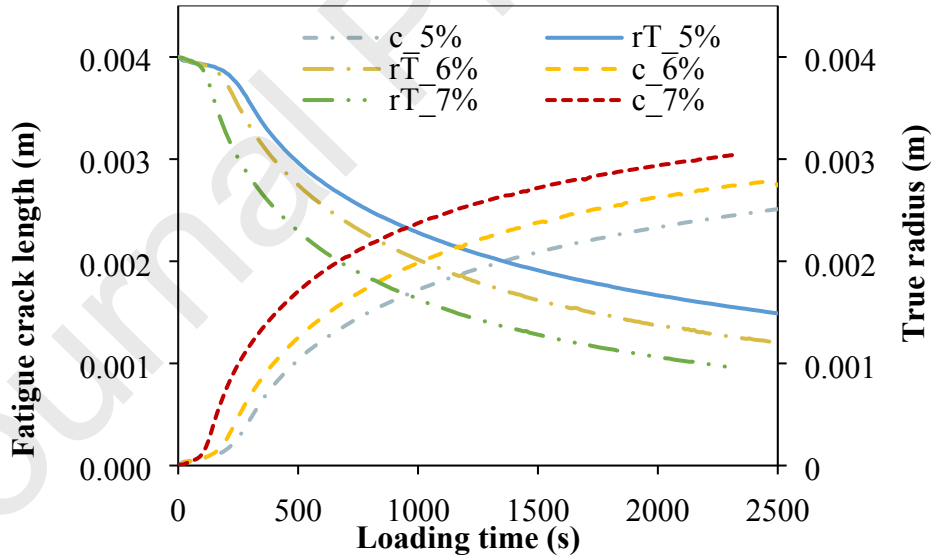


Fig.4. Fatigue crack length and true radius of the bituminous material BB at 20°C and 5%, 6% and 7% of strain levels

Taking the bituminous material BB as an example, Fig. 4 shows the fatigue crack length and true radius of the bituminous material BB at 20°C and 5%, 6% and 7% of strain levels. It can be seen from Fig. 4 that the fatigue crack length of the bituminous material BB gradually increases with the increase of loading time at 5%, 6% and 7% of strain levels, but the curve gradually flattens out. The shear

stress of the bituminous materials decreases with the accumulation of damage degree when performing the controlled-strain shear fatigue test, which makes the strain energy dissipation calculated by the shear stress and shear strain decrease with the increase of loading time. Then, the fatigue crack length of the bituminous material BB increases with the increase of strain levels at the same loading time, while the change trend of true radius is opposite. Because the larger strain level will produce larger strain energy dissipation at the same loading time, which accelerates the fatigue crack propagation of the materials. In addition, the bituminous material BB also has similar change rules under other temperature conditions and the bituminous material BM₁ and BM₂ also have similar change patterns under different conditions.

Next, the crack growth rate of bituminous materials is calculated. Before the calculation of the crack growth rate, the relationship between the reciprocal of the true radius $1/r^T$ and the loading time t is first studied. Taking the calculation results of the bituminous materials BB and BM₂ at 20°C as an example, Fig. 5 shows the relationship between the true radius $1/r^T$ and the loading time t at 20°C and 5%, 6%, 7% of strain levels. It is indicated that they have a high linear correlation at different strain levels, the R² are both larger than 0.99. The bituminous materials BB and BM₂ under other temperature conditions, and the bituminous material BM₁ under any loading conditions also have high linear correlations.

Therefore, the linear model of the true radius $1/r^T$ and loading time t can be established as follows:

$$\frac{1}{r^T} = pt + q \quad (18)$$

where p , q are the intercept and slope of the linear model, respectively. It is worth mentioning that the linear relation Eq. (18) is derived for polystyrene melts in the study [28], and these model parameters have physical interpretation.

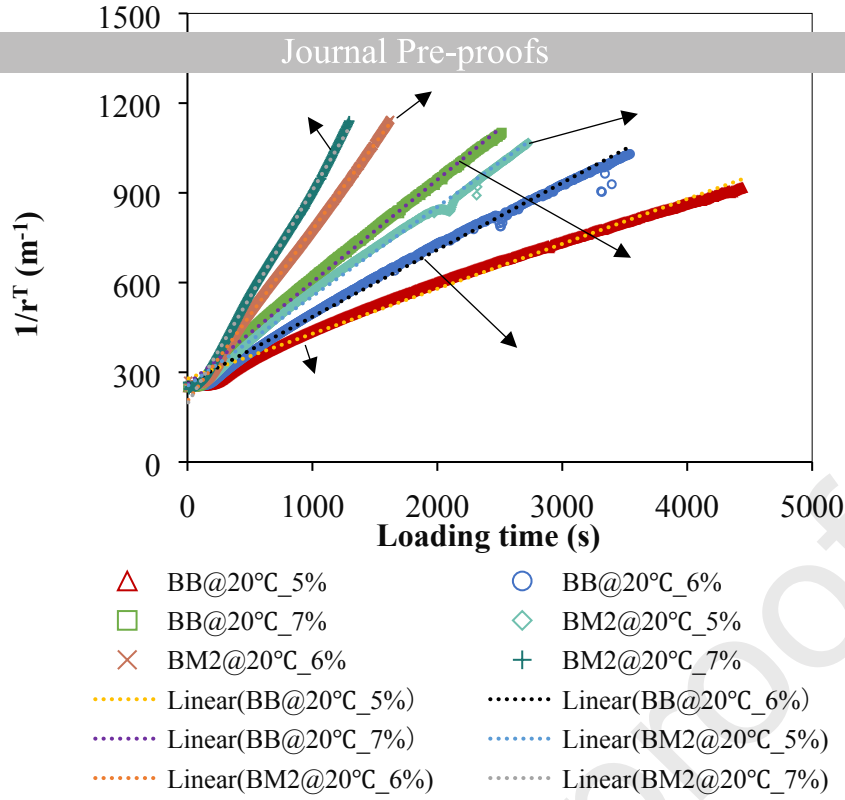


Fig.5. Relationship between the true radius $1/r^T$ and loading time t at 20°C and 5%, 6%, 7% of strain levels

Taking a derivative with respect to the loading time t in Eq. (18), which yield:

$$-\left(\frac{1}{r^T}\right)^2 \frac{dr^T}{dt} = p \quad (19)$$

Finally, the fatigue crack growth rate of bituminous materials can be obtained by differentiating the fatigue crack length with respect to the loading time t , and substituting Eq. (17) into Eq. (19) produce the following equation:

$$\frac{dc}{dt} = \frac{d(r^A - r^T)}{dt} = -\frac{dr^T}{dt} = p(r^T)^2 \quad (20)$$

Therefore, the fatigue crack growth rate of bituminous materials can be expressed as a function of the parameter p and the true radius r^T .

In this way, the fatigue crack growth rate of bituminous materials can be obtained based on the p value determined by the Eq. (18), and the true radius calculated by the Eq. (16). In addition, the fatigue crack growth rate of bituminous materials can also be calculated by the fatigue crack length increment of two adjacent loading time intervals $\Delta c / \Delta t$ (Δc is the increment of fatigue crack length and Δt is the increment of the loading time).

Taking the calculation results of the bituminous materials BB and BM₂ at 20°C and 5% of strain level as an example. Fig. 6 shows the relationship between $\ln(\Delta c / \Delta t)$, $\ln(dc/dt)$ and the loading time t . It can be seen from Fig. 6 that $\ln(dc/dt)$ cannot match

$\ln(\Delta c/\Delta t)$ at the initial loading stage, but after a certain loading time, they are well matched. This is because “edge unstable flow” exists at the initial loading stage of viscoelastic materials when performing the fatigue test [29-31], and the mechanism of the “edge unstable flow” is different from that of the fatigue crack growth. This study aims to establish a fatigue crack growth rate model for the stable fatigue crack growth stage, hence the “edge unstable flow” stage is not included. The result of $\ln(dc/dt)$ calculated by Eq. (20) has a good continuity, while the result of $\ln(\Delta c/\Delta t)$ has a large fluctuation during the late loading period. This is because the shear modulus during fatigue cracking process of bituminous materials fluctuates in the late loading period, which causes the variation of $\ln(\Delta c/\Delta t)$.

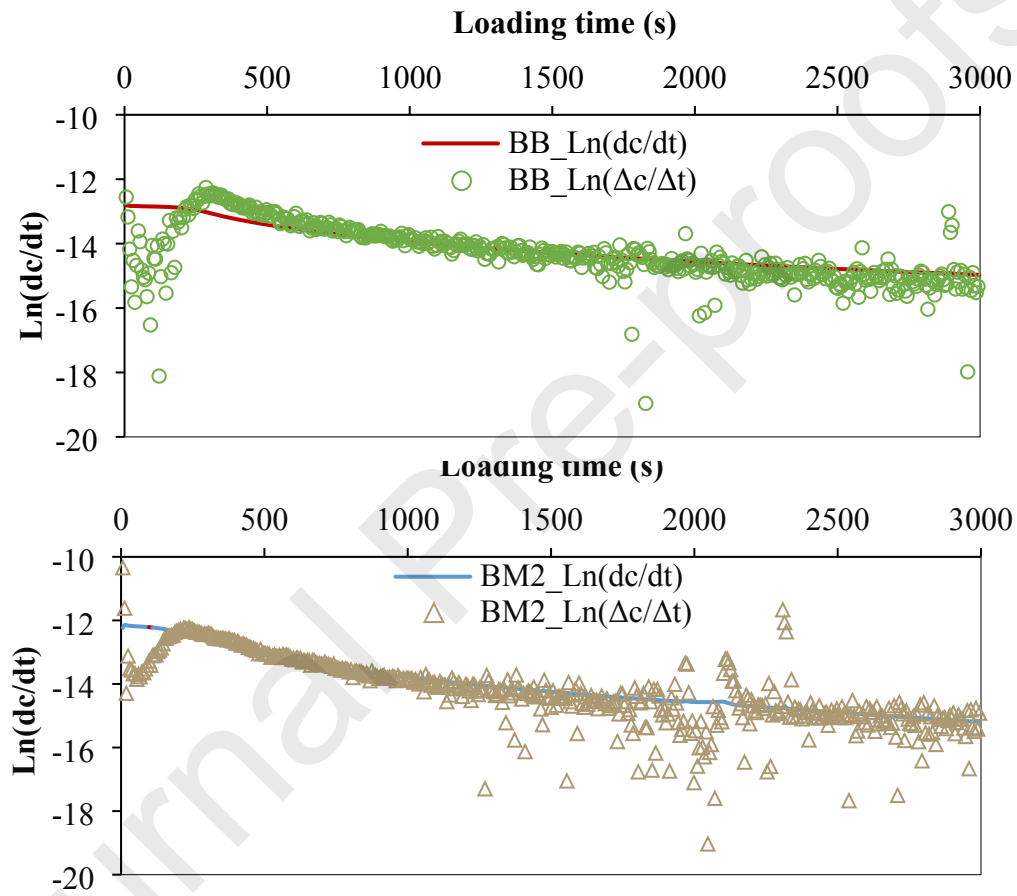


Fig.6. Relationship between $\ln(\Delta c/\Delta t)$, $\ln(dc/dt)$ and the loading time t

According to the analysis above, Eq. (20) can predict the fatigue crack growth rate for bituminous materials well. Therefore, in this study, the fatigue crack growth rates of bituminous materials at different temperatures, strain levels and damage degrees are calculated by Eq. (20). Fig. 7 shows the fatigue crack growth rates of the bituminous material BB, BM₁ and BM₂ at different temperatures and different crack lengths. Three observations can be drawn:

- 1) The fatigue crack growth rates of the bituminous material BB, BM₁ and BM₂ decrease with the increase of fatigue crack length.

The reason is that the energy dissipation caused by fatigue cracking decreases when performing the controlled-strain shear fatigue

test, so the fatigue crack growth rate decreases with the increase of fatigue crack length;

- 2) At the same fatigue crack length, the fatigue crack growth rate increases with the increase of the powder content. Because the powder will increase the “stiffness” for bituminous materials, which makes the energy dissipation caused by fatigue cracking increase at the same strain level; and
- 3) The fatigue crack growth rates of the bituminous materials BB, BM₁ and BM₂ decrease with the increase of temperature at the same strain level. Because bituminous materials become relatively "soft" at higher temperatures and "stiff" at lower temperatures, and the energy dissipation caused by fatigue cracking decreases at high temperatures when the strain level is same. Hence, the fatigue crack growth rate of bituminous materials at high temperature is lower than that at low temperature.

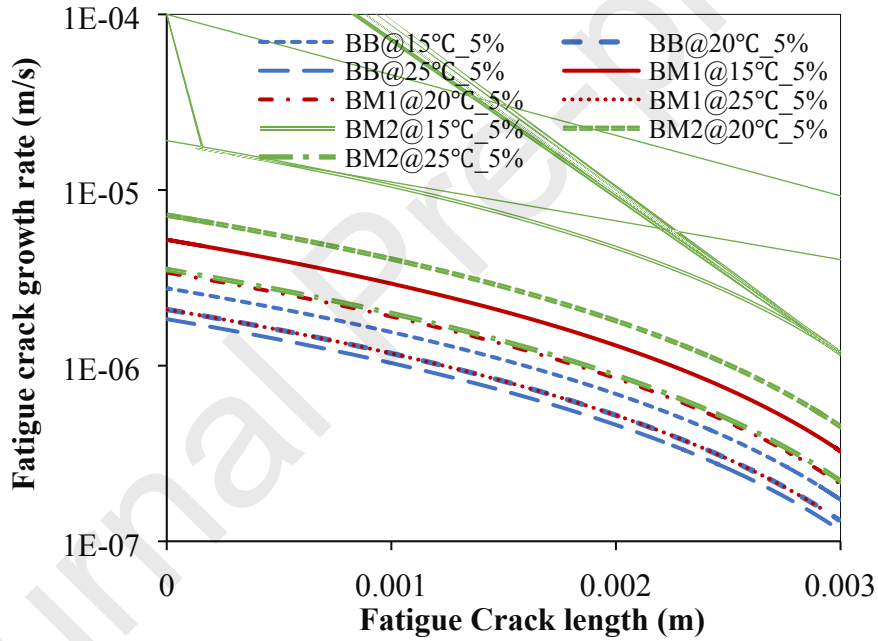


Fig.7. Relationship between the fatigue crack growth rate and fatigue crack length of the bituminous materials BB, BM₁ and BM₂

As a result, the fatigue crack growth rate of bituminous materials is related to temperature, strain level and damage degree. However, only the influence of damage degree (true radius r^T) on fatigue crack growth rate is included in Eq. (20). The p value in Eq. (20) is the intercept of the $1/r^T$ vs. the loading time t , which cannot directly reflect the influence of the temperature and strain level. In addition, it is not a coincidence that the value of $1/r^T$ of the bituminous materials BB, BM₁ and BM₂ have a highly linear relationship with the loading time t at all temperatures and strain levels. The authors believe that Eq. (20) must have a mechanism for the bituminous materials, and

4 Establishment of Kinetics-Based Model of Fatigue Crack Growth Rate

This section will focus on exploring the relationship between the p value and temperature and strain level. If the relationship between the p value and temperature, strain level is clearly presented, Eq. (20) will be expressed as a function of temperature, strain level and damage degree. Thus, Eq. (20) can be used to predict the fatigue crack growth rate at any temperature, strain level and damage degree for bituminous materials. To achieve it, this section contains the following four parts:

- (1) Solve the kinetic parameters (cracking activation energy and pre-exponential factor) characterizing the fatigue crack growth rate of bituminous materials based on the Arrhenius equation;
- (2) Analyze the cracking activation energy of bituminous materials based on the statistical analysis method;
- (3) Determine the cracking pre-exponential factor model of bituminous materials coupling with strain level and damage degree;
- (4) Establish the kinetic-based model of fatigue crack growth rate of bituminous materials coupling with temperature, strain level and damage degree.

4.1 Calculation of Kinetic Parameters of Fatigue Crack Growth Rate

The Arrhenius equation can be used to correlate a rate process with temperature. The authors have adapted the Arrhenius equation to establish correlation between the modulus change rate and the field temperature, and a kinetic aging prediction model which can characterize the aging process of the service asphalt pavements has been established [32-34]. In the kinetic theory, the rate constant k is usually used to evaluate how quickly any physical or chemical process reaches equilibrium. The rate constant k can be obtained by experiments. The minimum energy that causes the physical or chemical process to occur in the system is called activation energy. Different physical or chemical processes have different activation energies. The Arrhenius equation is used to establish the relationship between the rate constant and the activation energy of a certain process as follows [35]:

$$k = A_0 \exp\left(-\frac{E_a}{RT}\right) \quad (21)$$

in which k is the rate constant of the process; A_0 is the pre-exponential factor of the process; E_a is the activation energy of the process;

In this study, the fatigue crack growth rate of Eq. (20) is substituted into Eq. (21) as the rate constant k in the Arrhenius equation, which yields:

$$\frac{dc}{dt} = A_c \exp\left(-\frac{E_{ac}}{RT}\right) \quad (22)$$

where A_c is cracking pre-exponential factor of bituminous materials during fatigue crack growth process; and E_{ac} is cracking activation energy of bituminous materials during fatigue crack growth process.

Taking the logarithm of both sides of Eq. (22), which yields:

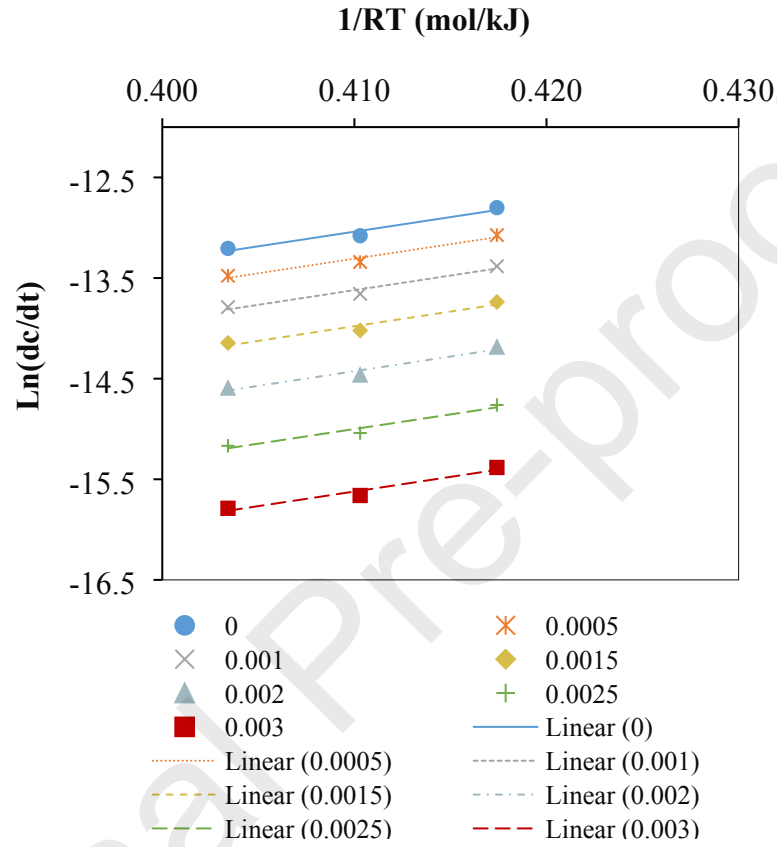
$$\ln\left(\frac{dc}{dt}\right) = \ln(A_c) - \frac{E_{ac}}{RT} \quad (23)$$

Eq. (23) derived from the Arrhenius equation demonstrates that $\ln(dc/dt)$ vs. $1/RT$ is linear function, and it is verified by using the experimental data. The $\ln(dc/dt)$ of bituminous materials at three temperatures (15°C, 20°C, 25°C), three strain levels (5%, 6%, 7%) and seven fatigue crack lengths (0, 0.0005m, 0.001m, 0.0015m, 0.002m, 0.0025m, 0.003m) are calculated based on the Eq. (20). Taking the 5% of strain level as an example, Fig. 8a, 8b and 8c present the relationship between $\ln(dc/dt)$ and $1/RT$ at 5% of strain level at different fatigue crack lengths for the bituminous material BB, BM₁ and BM₂, respectively. It indicates that there is a linear relationship between the $\ln(dc/dt)$ and $1/RT$ for the bituminous material BB, BM₁ and BM₂ at different fatigue crack lengths, and all of R² are greater than 0.95. It also presents strongly linear between $\ln(dc/dt)$ and $1/RT$ at other strain levels. Therefore, the correctness of Eq. (23) is validated by the experimental data. Furthermore, the slope E_{ac} and intercept $\ln(A_c)$ of $\ln(dc/dt)$ vs. $1/RT$ are the cracking activation energy and the natural logarithm of the cracking pre-exponential factor of bituminous materials, respectively. The E_{ac} , $\ln(A_c)$, and R² of the bituminous material BB, BM₁ and BM₂ are shown in Table 2.

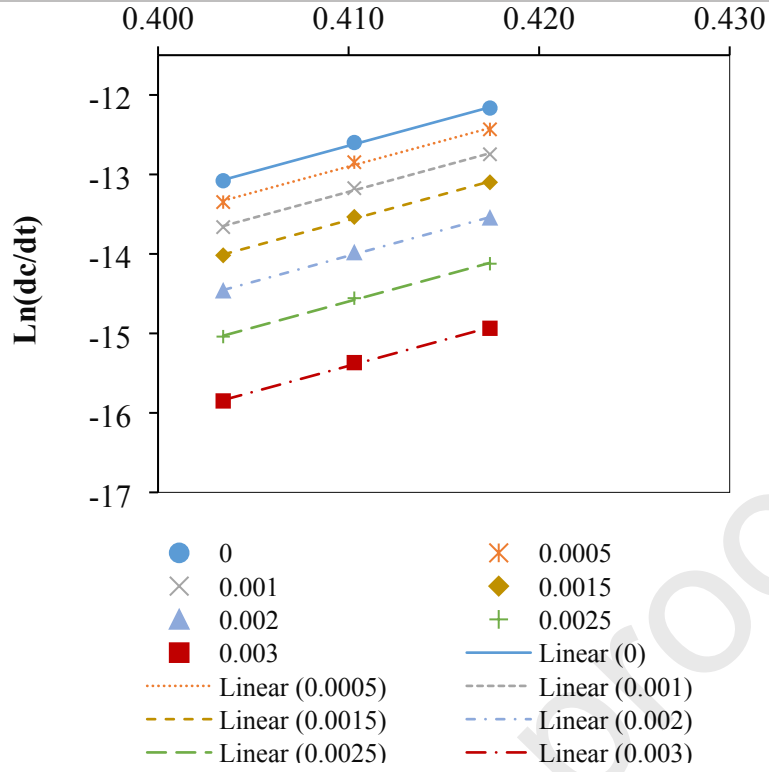
Table 2. E_{ac} , $\ln(A_c)$, and R² of the bituminous material BB, BM₁ and BM₂

Materials	Index	Fatigue crack length (m)						
		0	0.0005	0.001	0.0015	0.002	0.0025	0.003
BB	E_{ac}	29.0	28.9	29.1	29.2	29.1	29.0	29.0
	$\ln(A_c)$	-24.9	-25.2	-25.5	-25.9	-26.4	-26.9	-27.5
	R ²	0.959	0.970	0.965	0.955	0.962	0.959	0.960
BM ₁	E_{ac}	65.3	65.3	65.4	65.6	65.5	65.5	65.3

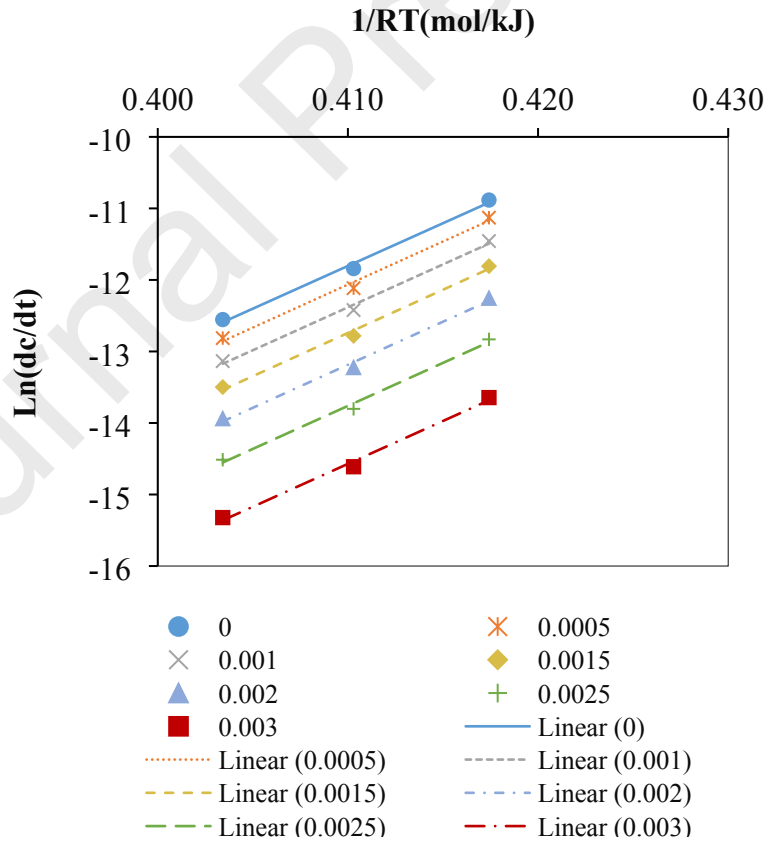
		Ln(A_c)	-39.4	-39.7	-40.0	-40.5	-40.9	-41.4	-42.2
		R^2	0.998	0.996	0.997	0.998	0.999	0.998	0.998
		E_{ac}	119.5	120.3	120.0	120.9	120.3	120.3	119.9
BM ₂	Ln(A_c)	-60.8	-61.4	-61.6	-62.3	-62.5	-63.1	-63.7	
	R^2	0.994	0.992	0.994	0.994	0.994	0.994	0.994	



a. Relationship between $\ln(dc/dt)$ and $1/RT$ at 5% of strain level at different fatigue crack lengths for the bituminous material BB



b. Relationship between $\ln(dc/dt)$ and $1/RT$ at 5% of strain level at different fatigue crack lengths for the bituminous material BM_1



c. Relationship between $\ln(dc/dt)$ and $1/RT$ at 5% of strain level at different fatigue crack lengths for the bituminous material BM_2

Fig.8. Relationship between $\ln(dc/dt)$ and $1/RT$ at 5% of strain level at different fatigue crack lengths for the bituminous material

4.2 Analyses of Cracking Activation Energy by Statistical Analysis Method

The cracking activation energy at different strain levels and fatigue crack lengths of the bituminous material BB, BM₁ and BM₂ shown in Table 2 are plotted together in Fig. 9. It can be seen from Fig. 9 that the cracking activation energy of bituminous materials increases with the increase of the powder content. The interaction between the bituminous binder and limestone powder is strengthened with the increase of the limestone powder content, and a larger cracking activation energy is required to force the bituminous material to crack. Therefore, the greater the cracking activation energy is, the better the fatigue cracking resistance of bituminous materials is, and vice versa. In addition, the cracking activation energies of the same material at different fatigue crack lengths and strain levels are close to each other.

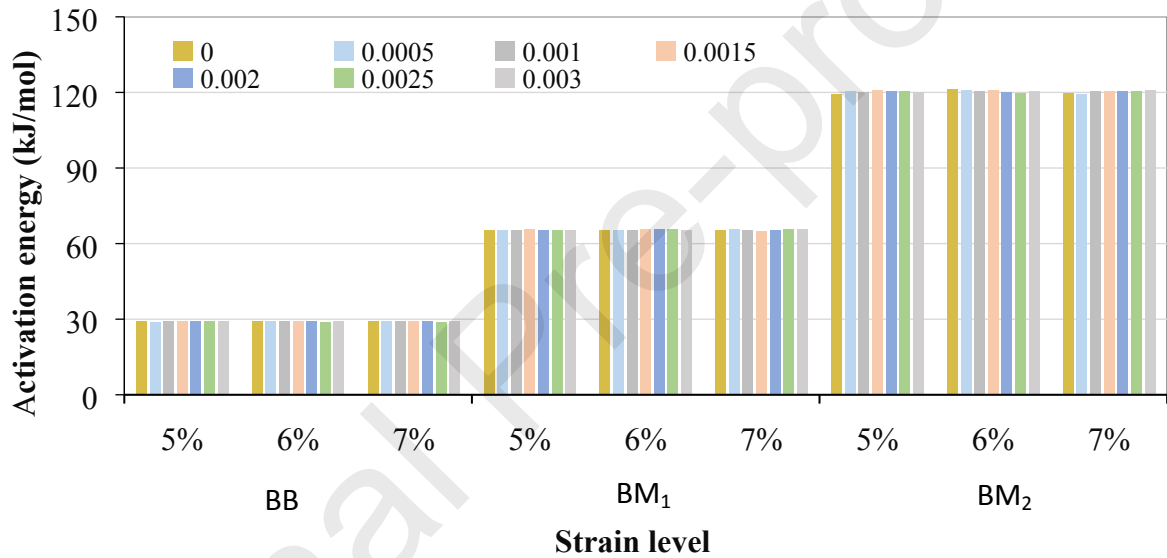


Fig.9. Cracking activation energy at different strain levels and different fatigue crack lengths of the bituminous material BB, BM₁ and

BM₂

In this section, to verify whether the cracking activation energy of bituminous materials changes with the change of external factors, the cracking activation energies of two repeated tests were obtained at seven fatigue crack lengths (0, 0.0005m, 0.001m, 0.0015m, 0.002m, 0.0025m, 0.003m) and three strain levels (5%, 6%, 7%). Next, the statistical analysis for the cracking activation energy at different strain levels and different fatigue crack lengths of the bituminous material BB, BM₁ and BM₂ are conducted. Since the cracking activation energy includes two influence factors, i.e., strain level and fatigue crack length, a Two-Way ANOVA is conducted in this study. The specific analysis process is as follows:

The Two-Way ANOVA in the data analysis module of Microsoft EXCEL software is used for statistical analysis for hypothesis I and II. Analysis results of the bituminous material BB, BM_1 and BM_2 are shown in Table 4. It shows that the F- statistic of the three bituminous materials at different strain levels and different crack lengths are correspondingly greater than the F- critical statistic, and the P - values are greater than 0.05 when the confidence level is 95%. It indicates that the cracking activation energies at different strain levels and different fatigue crack lengths of bituminous materials have no significant difference. Therefore, the cracking activation energy is independent on the external factors, i.e., it can be used as an inherent material parameter. Thus, the cracking activation energy can be used as a characteristic property to evaluate the anti-cracking performance for bituminous materials.

Table 3 Null hypothesis and alternative hypothesis for statistical hypothesis testing

Hypothesis	Null hypothesis H_0	Alternative hypothesis H_1
I	$E_{ac}^{\gamma_1} = E_{ac}^{\gamma_2} = E_{ac}^{\gamma_3}$	At least one E_{ac} differs from the rest
II	$E_{ac}^{c_1} = E_{ac}^{c_2} = E_{ac}^{c_3} = E_{ac}^{c_4} = E_{ac}^{c_5} = E_{ac}^{c_6} = E_{ac}^{c_7}$	

Table 4 Values of the F-statistic and critical F-statistic of Two-Way ANOVA test at 95% confidence level

Materials	Influence factor	F-statistic	P-value	F-critical statistic
BB	Strain level	1.820	0.178	2.996
	Fatigue crack length	1.347	0.297	3.885

		0.681	0.669	2.996
	Strain level	0.681	0.669	2.996
	Fatigue crack length	0.003	0.997	3.885
	Strain level	0.427	0.847	2.996
BM ₂	Fatigue crack length	0.922	0.424	3.885

4.3 Determination of Cracking Pre-exponential Factor Model

It is proved that the cracking activation energy of bituminous materials is independent of the strain level and damage degree by the Two-Way ANOVA. Next, the analysis of another key indicator in the Arrhenius equation, the cracking pre-exponential factor, is analyzed in this section. As shown in Table 2, the cracking pre-exponential factors of the bituminous material BB, BM₁ and BM₂ at different strain levels decrease with the increase of the fatigue crack length. Because the cracking activation energy is only related to the material, the higher the cracking pre-exponential factor is, the larger the fatigue crack growth rate of the bituminous materials will be. In addition, Fig. 10a, 10c and 10e show the scatter diagram of $\ln(A_c)$ vs. true radius of the bituminous material BB, BM₁ and BM₂ at different strain levels, respectively. The results show that the $\ln(A_c)$ increases with the increase of the true radius (with the decrease of the fatigue crack length) of bituminous material. At the same true radius (or fatigue crack length), all of $\ln(A_c)$ of bituminous materials increase with the increase of strain level. Because the energy dissipation caused by fatigue cracking increases with the increase of strain level when the other loading conditions are same, so the fatigue crack growth rate increases with the increase of strain level when performing the controlled-strain fatigue test.

As a result, $\ln(A_c)$ in Eq. (23) is closely related to the strain level and true radius (fatigue crack length). $\ln(A_c)$ has similar change rules at different strain levels with the evolution of damage degree as shown in Fig. 10a, 10c and 10e. In this section, in order to establish the model of the cracking pre-exponential factor at different strain levels and damage degree, the shift factor of the true radius is first introduced, which is defined as follows:

$$\alpha^\gamma = \gamma / \gamma_r \quad (24)$$

where γ is a certain strain level for bituminous materials; and γ_r is a reference strain level for bituminous materials.

In this study, the strain levels of destructive time sweep tests of the bituminous materials are 5%, 6% and 7% respectively. The strain level of 6% is selected as an example for analysis. The same analysis procedure is performed for reference strain level of 5% or 7%, but

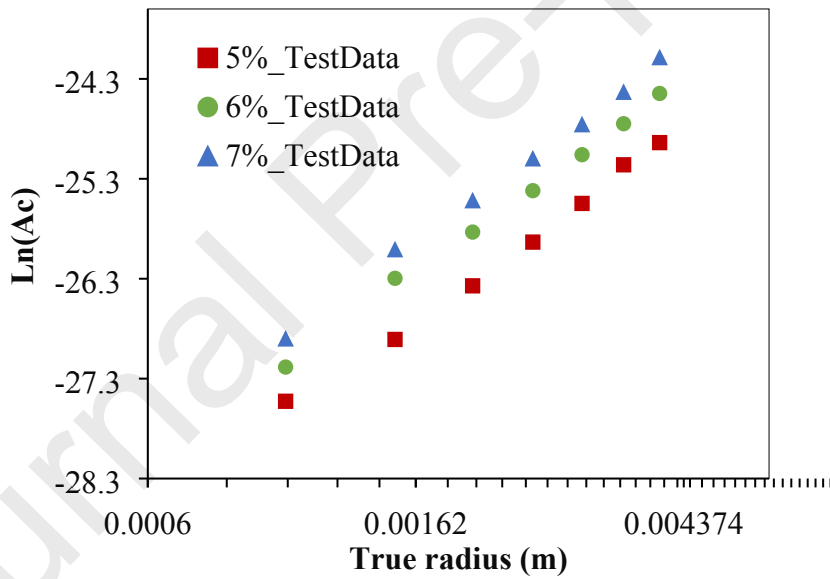
the shift factor is different. The strain levels of 5%, 6% and 7% are substituted into Eq. (24) to calculate the shift factor of the true radius at different strain levels, and then calculate $\alpha^\gamma r^T$. The relationship between $\ln(A_c)$ and $\ln(\alpha^\gamma r^T)$ of the bituminous material BB, BM₁ and BM₂ are shown in Fig. 10b, 10d and 10f, respectively.

When a linear equation is used to match the test data, it is found that $\ln(A_c)$ of the bituminous material BB, BM₁ and BM₂ present a good linear correlation with $\ln(\alpha^\gamma r^T)$ at different strain levels, and all of R² are greater than 0.95. Therefore, the linear equation is adopted to establish the relationship between $\ln(A_c)$ and $\ln(\alpha^\gamma r^T)$, as below:

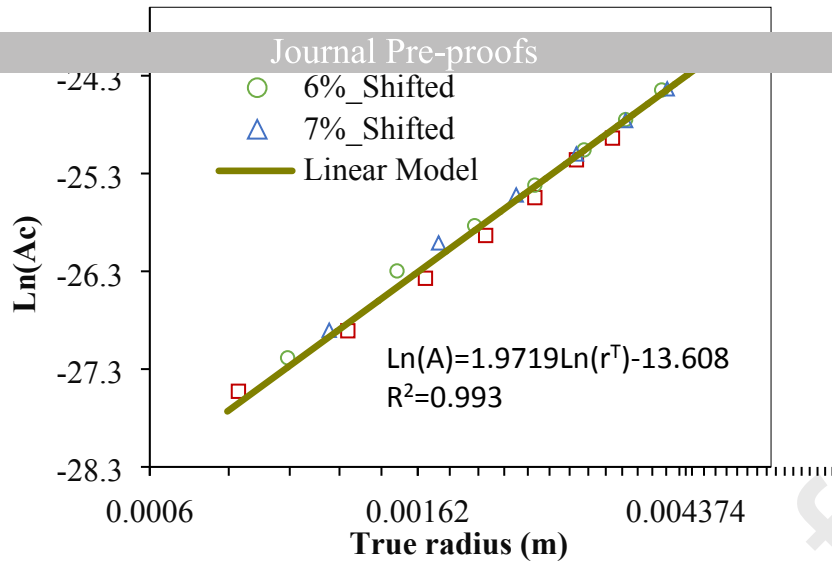
$$\ln(A_c) = a \ln(\alpha^\gamma r^T) + b \quad (25)$$

in which a , b are the model parameters of the cracking pre-exponential factor. Substituting Eq. (24) into Eq. (25), the model of the cracking pre-exponential factor related to strain level and damage degree of bituminous materials is obtained:

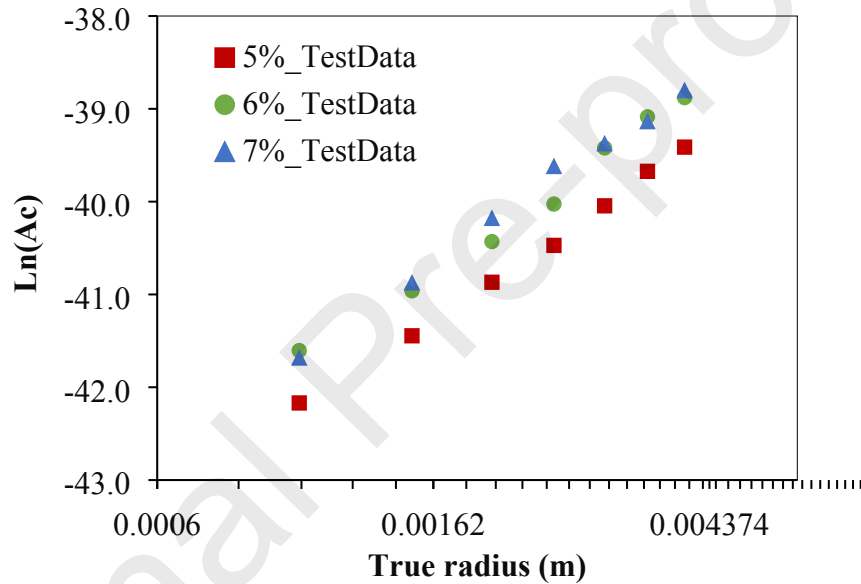
$$A_c = e^b \left(r^T \gamma / \gamma_r \right)^a \quad (26)$$



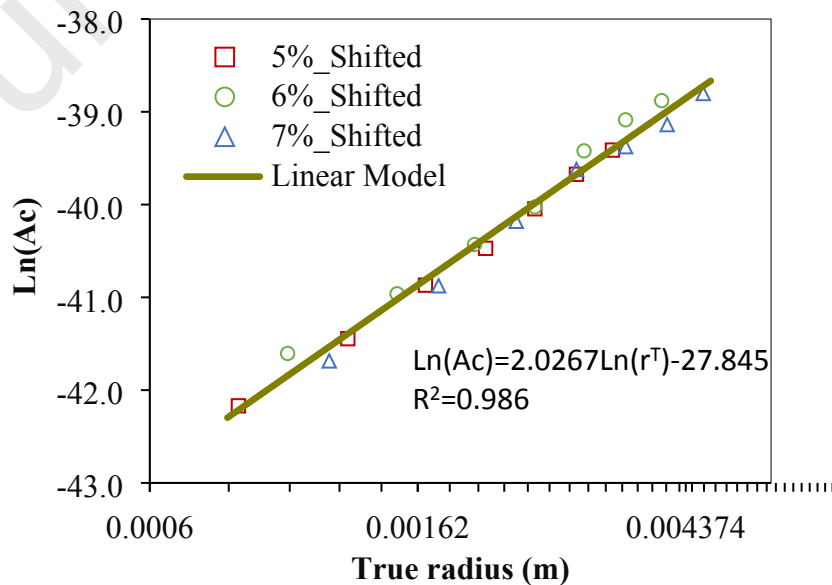
a. Scatter diagram of $\ln(A_c)$ vs. true radius of the bituminous material BB at different strain levels



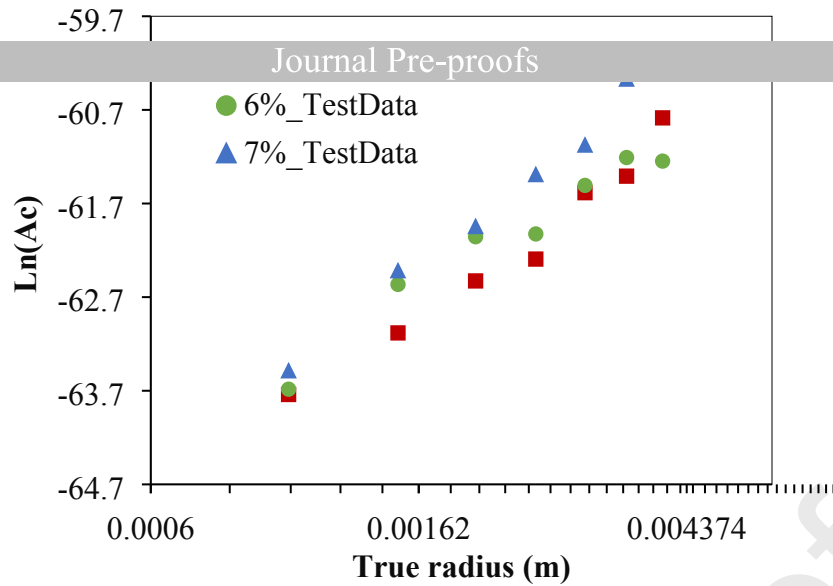
b. Relationship between $\text{Ln}(A_c)$ and $\text{Ln}(\alpha^r r^T)$ of the bituminous material BB



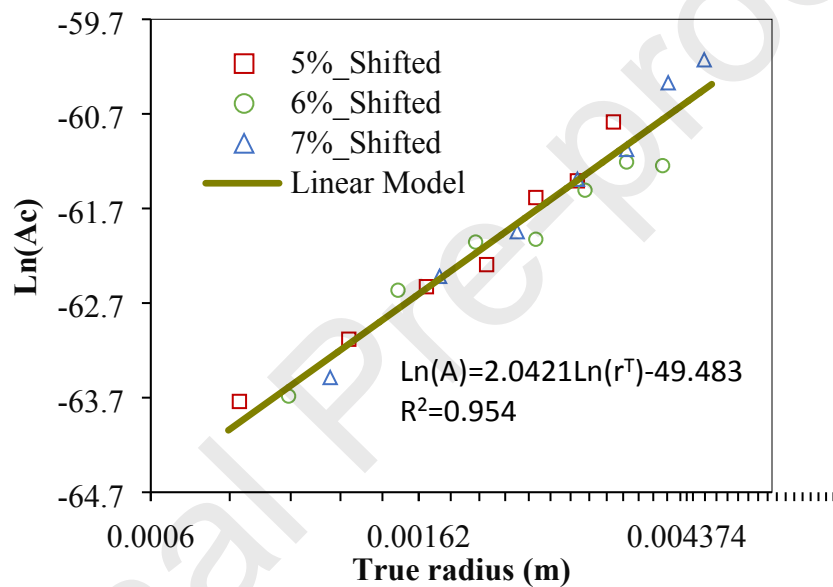
c. Scatter diagram of $\text{Ln}(A_c)$ vs. true radius of the bituminous material BM_1 at different strain levels



d. Relationship between $\text{Ln}(A_c)$ and $\text{Ln}(\alpha^r r^T)$ of the bituminous material BM_1



e. Scatter diagram of $\ln(A_c)$ vs. true radius of the bituminous material BM_2 at different strain levels



f. Relationship between $\ln(A_c)$ and $\ln(\alpha^\gamma r^T)$ of the bituminous material BM_2

Fig.10. Scatter diagram of $\ln(A_c)$ vs. true radius, relationship between $\ln(A_c)$ and $\ln(\alpha^\gamma r^T)$ of the bituminous material BB , BM_1 and BM_2 at different strain levels

4.4 Establishment of Kinetic-Based Model of Fatigue Crack Growth Rate

The cracking activation energy and the cracking pre-exponential factor of bituminous materials are analyzed above. The kinetic-based model of fatigue crack growth rate of bituminous materials coupling with temperature, strain level and damage degree is established in this section. First, the parameters a , b in the cracking pre-exponential factor model are analyzed. Fig. 11 presents the relationship between parameters a , b and the cracking activation energy. It indicates that the parameter a almost does not change with the change

of the cracking activation energy which can be regarded as a constant of 2. This is the same power as in the crack growth rate model

$dc/dt = p(r^T)^2$. The parameter b decreases linearly with the increase of the cracking activation energy, and the linear model is

$b = -0.3933E_a - 2.1539$, $R^2=1$. In this way, the parameter a in Eq. (25) is constant 2, and the parameter b is only related to the

material, which can be determined by the cracking activation energy of the bituminous material.

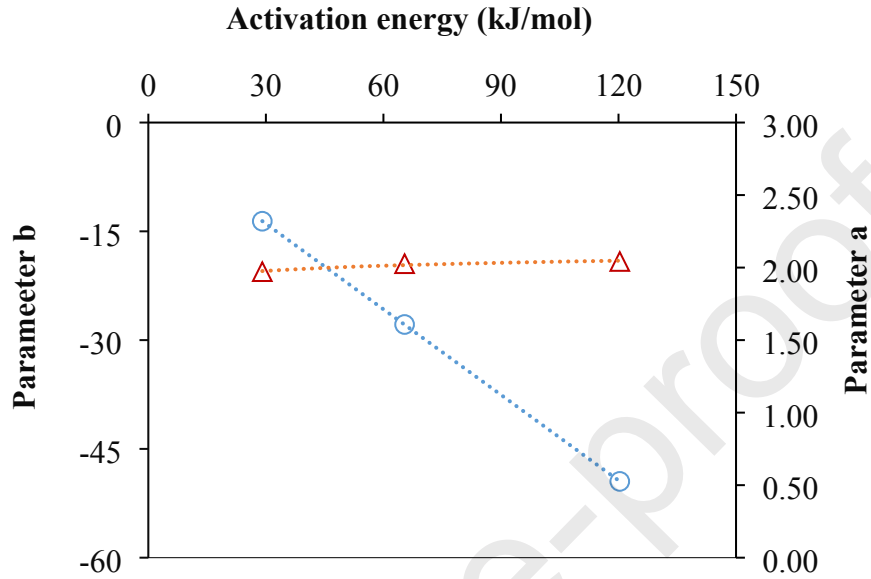


Fig.11. Relationship between the parameters a , b and the cracking activation energy

Substituting Eq. (26) into Eq. (22), yields:

$$\frac{dc}{dt} = e^b (\gamma / \gamma_r)^a \exp(-E_a / RT) (r^T)^a \quad (27)$$

The comparison between Eq. (27) and Eq. (20) shows that $p = e^b (\gamma / \gamma_r)^a \exp(-E_a / RT)$. Therefore, p value is associated with the strain level, temperature, and cracking activation energy.

Finally, substituting Eq. (17) into Eq. (27), the kinetic-based model of fatigue crack growth rate of bituminous materials coupling with temperature, strain level and damage degree can be established, which is present as below:

$$\frac{dc}{dt} = e^b (\gamma / \gamma_r)^a \exp(-E_a / RT) (r^A - c)^2 = f(\gamma, \gamma_r, E_a, T, c) \quad (28)$$

In this way, the fatigue crack growth rate of the bituminous materials at arbitrary temperature, strain level, and damage degree can be predicted by Eq. (28).

5 Conclusions and Future Work

The fatigue crack growth rate of bituminous materials is a crucial indicator to evaluate the failure rate during the fatigue crack propagation process. Based on the EBM approach and Arrhenius equation, the kinetic-based model of fatigue crack growth rate of bituminous materials coupling with temperature, strain level and damage degree has been established in this study. The main conclusions are as follows:

- The fatigue crack growth rate of bituminous materials increases with the increase of the powder content, increases with the decrease of the temperature, increases with the increase of the strain level, and decreases with the increase of the fatigue crack length when performing the controlled-strain fatigue test.
- The reciprocal of the true radius of bituminous materials is linearly related to the loading time at any temperature and strain level, and the logarithm of fatigue crack growth rate is linear to the inverse of the absolute temperature at any strain levels.
- The cracking activation energy of bituminous materials is independent on strain level and damage degree. It can be regarded as an inherent material parameter. The greater the cracking activation energy is, the better the fatigue cracking resistance of bituminous materials is, and vice versa. It can be used as a characteristic indicator to evaluate the fatigue cracking resistance for bituminous materials.
- The cracking pre-exponential factor of bituminous materials is a function of strain level, damage degree and cracking activation energy. In addition, the kinetic-based model of fatigue crack growth rate of bituminous materials coupling with temperature, strain level and damage degree is proposed, which can predict the fatigue crack growth rate at arbitrary temperature, strain level, and damage degree.

In the future, the cohesive cracking of the bituminous binder and adhesive cracking between the bituminous binder and mineral powder will be separated by the mechanics theory when performing the fatigue test. Then, determining the surface energy of the bituminous binder and mineral powder based on the proportion of the cohesive cracking and adhesive cracking. In addition, the relationship between the cracking activation energy and surface energy of the bituminous binder and mineral powder will be investigated. It will be helpful to further reveal the physical interpretation of fatigue and contribute to better modeling and prediction for the bituminous material.

Reference

- [1] Cheng, D. X., Little, D., Lytton, R., & Holste, J. (2002). Surface energy measurement of asphalt and its application to predicting

44-53.

- [2] Azarhoosh, A. R., Nejad, F. M., & Khodaii, A. (2016). The influence of cohesion and adhesion parameters on the fatigue life of hot mix asphalt. *The Journal of Adhesion*, 1-20.
- [3] Hicks, R. G., Finn, F. N., Monismith, C. L., & Leahy, R. B. (1993). Validation of SHRP binder specification through mix testing (with discussion). *Journal of the Association of Asphalt Paving Technologists*, 62.
- [4] Kim, Y. R., Lee, H. J., & Little, D. N. (1997). Fatigue characterization of asphalt concrete using viscoelasticity and continuum damage theory (with discussion). *Journal of the Association of Asphalt Paving Technologists*, 66.
- [5] Reese, R. (1997). Properties of aged asphalt binder related to asphalt concrete fatigue life. *Journal of the Association of Asphalt Paving Technologists*, 66.
- [6] Rowe, G. M., & Bouldin, M. G. (2000). Improved techniques to evaluate the fatigue resistance of asphaltic mixtures. In *2nd Eurasphalt & Eurobitume Congress Barcelona* (Vol. 2000).
- [7] Zhou, F., Mogawer, W., Li, H., Andriescu, A., & Copeland, A. (2013). Evaluation of fatigue tests for characterizing asphalt binders. *Journal of Materials in Civil Engineering*, 25 (5), 610-617.
- [8] Anderson, D. A., Le Hir, Y. M., Marasteanu, M. O., Planche, J. P., Martin, D., & Gauthier, G. (2001). Evaluation of fatigue criteria for asphalt binders. *Transportation Research Record*, 1766 (1), 48-56.
- [9] Ghuzlan, K. A., & Carpenter, S. H. (2000). Energy-derived, damage-based failure criterion for fatigue testing. *Transportation research record*, 1723 (1), 141-149.
- [10] Wang, C., Zhang, H., Castorena, C., Zhang, J., & Kim, Y. R. (2016). Identifying fatigue failure in asphalt binder time sweep tests. *Construction and Building Materials*, 121, 535-546.
- [11] Carpenter, S. H., & Jansen, M. (1997). Fatigue behavior under new aircraft loading conditions. In *Aircraft/Pavement Technology in the Midst of Change ASCE, Air Transport Division, Airfield Pavement Committee American Society of Civil Engineers*.
- [12] Shen, S., Airey, G. D., Carpenter, S. H., & Huang, H. (2006). A dissipated energy approach to fatigue evaluation. *Road materials and pavement design*, 7 (1), 47-69.

- [13] Shen, S., Chiu, H. M., & Huang, H. (2010). Characterization of fatigue and healing in asphalt binders. *Journal of Materials in Civil Engineering*, 22 (9), 846-852.
- [14] Subhy, A., Presti, D. L., & Airey, G. (2017). New simplified approach for obtaining a reliable plateau value in fatigue analysis of bituminous materials. *Engineering Failure Analysis*, 79, 263-273.
- [15] Anderson, D. A., & Kennedy, T. W. (1993). Development of SHRP binder specification (with discussion). *Journal of Association of Asphalt Paving Technologists*, 62, 481-507.
- [16] Mannan, U. A., & Tarefder, R. A. (2018). Investigating different fatigue failure criteria of asphalt binder with the consideration of healing. *International Journal of Fatigue*, 114, 198-205.
- [17] Shan, L. Y., Tan, Y. Q., & Xu, Y. N. (2016). Fatigue damage evolution rules of asphalt under controlled-stress and controlled-strain modes. *China Journal of Highway and Transport*, 29(1), 16-21.
- [18] Shan, L., Tian, S., He, H., & Ren, N. (2017). Internal crack growth of asphalt binders during shear fatigue process. *Fuel*, 189, 293-300.
- [19] Hintz, C., & Bahia, H. (2013). Understanding mechanisms leading to asphalt binder fatigue in the dynamic shear rheometer. *Road Materials and Pavement Design*, 14 (sup2), 231-251.
- [20] Li, H., Luo, X., Yan, W., & Zhang, Y. (2020). Energy-Based Mechanistic Approach for Crack Growth Characterization of Asphalt Binder. *Mechanics of Materials*, 103462.
- [21] Li, H., Luo, X., Yan, W., & Zhang, Y. (2020). Pseudo Energy-based Kinetic Characterization of Fatigue in Asphalt Binders. *China Journal of Highway and Transport*, 2020, 33(10): 115-124.
- [22] Luo, X., Zhang, Y., & Lytton, R. L. (2016). Implementation of pseudo J-integral based Paris' law for fatigue cracking in asphalt mixtures and pavements. *Materials and Structures*, 49(9), 3713-3732.
- [23] Zhang, Y., Gu, F., Birgisson, B., & Lytton, R. L. (2018). Modelling cracking damage of asphalt mixtures under compressive monotonic and repeated loads using pseudo J-integral Paris' law. *Road Materials and Pavement Design*, 19(3), 525-535.
- [24] Gao, Y., Li, L., & Zhang, Y. (2020). Modeling Crack Propagation in Bituminous Binders under a Rotational Shear Fatigue Load using Pseudo J-Integral Paris' Law. *Transportation Research Record*, 2674(1), 94-103.

- [25] Luo, X., Luo, R., & Lytton, R. L. (2014). Energy-based mechanistic approach for damage characterization of pre-flawed visco-elasto-plastic materials. *Mechanics of Materials*, 70, 18-32.
- [26] Luo, X., Li, H., Deng, Y., & Zhang, Y. (2020). Energy-Based Kinetics Approach for Coupled Viscoplasticity and Viscofracture of Asphalt Mixtures. *Journal of Engineering Mechanics*, 146(9), 04020100.
- [27] Luo, X., Birgisson, B., & Lytton, R.L. (2020). Kinetics of healing of asphalt mixtures. *Journal of Cleaner Production*, 252, 119790.
- [28] Mattes, K. M., Vogt, R., & Friedrich, C. (2008). Analysis of the edge fracture process in oscillation for polystyrene melts. *Rheologica acta*, 47(8), 929-942.
- [29] Keentok, M., Xue, S.C., 1999. Edge fracture in cone-plate and parallel plate flows. *Rheologica Acta* 38 (4), 321–348.
- [30] Anderson, D., Hir, Y., Marasteanu, M., Planche, J. P., Martin, D., & Gauthier, G. (2001). Evaluation of fatigue criteria for asphalt binders. *Transportation Research Record Journal of the Transportation Research Board*, 1766, 48-56.
- [31] Gao, Y., Li, L., & Zhang, Y. (2020). Modelling crack initiation in bituminous binders under a rotational shear fatigue load. *International Journal of Fatigue*, 105738.
- [32] Luo, X., Gu, F., & Lytton, R. L. (2015). Prediction of field aging gradient in asphalt pavements. *Transportation Research Record: Journal of the Transportation Research Board*, 2507(1), 19-28.
- [33] Luo, X., Gu, F., & Lytton, R. L. (2017). Kinetics-based aging prediction of asphalt mixtures using field deflection data. *International Journal of Pavement Engineering*, 1-11.
- [34] Luo, X., Gu, F., Zhang, Y., Lytton, R. L., & Birgisson, B. (2018). Kinetics-based aging evaluation of in-service recycled asphalt pavement. *Journal of Cleaner Production*, 200, 934-944.
- [35] Bamford, C. H. and Tipper, C. F. H. eds. (1969). *Comprehensive Chemical Kinetics: The theory of kinetics (Vol. 2)*. Elsevier Scientific Publishing Company, Amsterdam, The Netherlands.

Declaration of Interest

The authors declare that they have no conflict of interest.

Journal Pre-proofs

Highlights

Logarithm of fatigue crack growth rate is linear to the inverse of absolute temperature

Cracking activation energy is independent on strain level and damage degree

A kinetics-based model of fatigue crack growth rate is proposed

Journal Pre-proofs